Soft Matter

PAPER

View Article Online
View Journal | View Issue

Cite this: *Soft Matter*, 2016, 12, 9692

Adsorption and desorption behavior of ionic and nonionic surfactants on polymer surfaces†

Giulia Magi Meconi,[a] Nicholas Ballard,[a] José M. Asua[a] and Ronen Zangi*[bc]

We report combined experimental and computational studies aiming to elucidate the adsorption properties of ionic and nonionic surfactants on hydrophobic polymer surface such as poly(styrene). To represent these two types of surfactants, we choose sodium dodecyl sulfate and poly(ethylene glycol)–poly(ethylene) block copolymers, both commonly utilized in emulsion polymerization. By applying quartz crystal microbalance with dissipation monitoring we find that the non-ionic surfactants are desorbed from the poly(styrene) surface slower, and at low surfactant concentrations they adsorb with stronger energy, than the ionic surfactant. If fact, from molecular dynamics simulations we obtain that the effective attractive force of these nonionic surfactants to the surface increases with the decrease of their concentration, whereas, the ionic surfactant exhibits mildly the opposite trend. We argue that the difference in this contrasting behavior stems from the physico-chemical properties of the head group. Ionic surfactants characterized by small and strongly hydrophilic head groups form an ordered self-assembled structure at the interface whereas, non-ionic surfactants with long and weakly hydrophilic head groups, which are also characterized by low persistence lengths, generate a disordered layer. Consequently, upon an increase in concentration, the layer formed by the nonionic surfactants prevents the aprotic poly(ethylene glycol) head groups to satisfy all their hydrogen bonds capabilities. As a response, water molecules intrude this surfactant layer and partially compensate for the missing interactions, however, at the expense of their ability to form hydrogen bonds as in bulk. This loss of hydrogen bonds, either of the head groups or of the intruding water molecules, is the reason the nonionic surfactants weaken their effective attraction to the interface with the increase in concentration.

Received 14th August 2016,
Accepted 10th November 2016

DOI: 10.1039/c6sm01878e

www.rsc.org/softmatter

Introduction

Surfactants are employed in a wide range of applications, from soaps and detergents to anti-corrosion and anti-static agents. There are all characterized by their ability to reduce the tension of the surface (or interface) on which they are adsorbed. The reduction in the surface tension, γ (or in the free energy per surface area), relative to the change in the chemical potential of the surfactant, $\mu_{\text{surfactant}}$, is given by the Gibbs adsorption isotherm,[1]

$$\frac{\mathrm{d}\gamma}{\mathrm{d}\mu_{\text{surfactant}}} = -\Gamma \qquad (1)$$

and it equals the excess (relative to bulk) number of surfactants, per unit area, at the surface, Γ.

The adsorption of surfactants to solid or liquid interfaces has also long been used as a means to stabilize various colloidal dispersions by providing repulsive electrostatic and/or steric interactions which prevent aggregation. The chemical identity of the surfactant head group, which provides colloidal stability, predominantly determines the surfactant properties and its classification. In fact, the difference in the behavior of ionic surfactants compared with that of nonionic surfactants, as encountered in the process of emulsion polymerization, is where our interest in the current work arises. Emulsion polymerization is an industrial process developed in the middle of the 20th century for the production of dispersed polymers that are applied in numerous commercial applications. While significant steps have been made in the fundamental understanding of this process and its use in producing high quality materials, the underlying formulation, consisting of water, oil soluble monomer(s), initiator and surfactant remains the same as that applied 70 years ago.[2] The presence of surfactant is often considered a necessary evil in that it tends to affect negatively the physical performance of the final polymer. Nevertheless, its presence in the formulation is vital in order to prevent particle aggregation and coagulation in the reactor.

[a] POLYMAT & Departamento de Química Aplicada, Facultad de Ciencias Químicas, University of the Basque Country UPV/EHU, Avenida de Tolosa 72, 20018, Donostia-San Sebastián, Spain
[b] POLYMAT & Departamento de Química Orgánica I, University of the Basque Country UPV/EHU, Avenida de Tolosa 72, 20018, Donostia-San Sebastián, Spain
[c] IKERBASQUE, Basque Foundation for Science, María Díaz de Haro 3, 48013 Bilbao, Spain. E-mail: r.zangi@ikerbasque.org

† Electronic supplementary information (ESI) available. See DOI: 10.1039/c6sm01878e

Furthermore, the presence of surfactant also plays a defining role in the kinetics of particle nucleation during the polymerization process, and therefore, also heavily affects the rate of polymerization.[3,4]

Despite the importance of surfactants in the emulsion polymerization process, they are still largely employed based on empirical observations of their behavior. For example, ionic surfactants are known to nucleate particles efficiently but the final latex tends to exhibit poor freeze–thaw stability and films cast from the polymer dispersion have increased sensitivity to water. In contrast, nonionic surfactants are much better at stabilizing the latex, particularly with regard to freeze–thaw stability, and have fewer negative effects on the physical properties of the final product whilst being less efficient at nucleating particles. Therefore, in order to optimize the properties of the surfactant in both the reactor and in the final product it is common to use a mixture of ionic and nonionic surfactants.

In this work we seek to take a deeper look at how surfactants interact with polymer surfaces, so that we better understand their effects on the emulsion polymerization process. As a model for ionic surfactants we consider sodium dodecyl sulfate (SDS) and for nonionic surfactants block copolymers of poly(ethylene oxide) (PEO) and poly(ethylene) (PE). These are among the most abundantly used surfactants, in general, and in emulsion polymerization in particular. Using quartz crystal microbalance with dissipation monitoring (QCM-D) we find that, at low surfactant concentrations, it is easier to desorb (as measured by the rate) ionic surfactants than nonionic surfactants. To the best of our knowledge this phenomenon has never been addressed before and no explanation for the difference in the behavior of the adsorption/desorption between ionic and nonionic surfactants has been proposed. In order to rationalize this observation we perform molecular dynamics (MD) simulations and calculate the reversible work necessary to remove one of these surfactants from the surface. Here we find that the work increases as the concentration of the nonionic surfactants at the surface decreases. In contrast, for ionic surfactants a moderate augmentation of the work is obtained with an increase in concentration. The reason for this opposing behavior is that with increasing concentration, the nonionic surfactants at the surface are increasingly less stable whereas no such destabilization is observed for ionic surfactants. We attribute these different trends to the physico-chemical properties of the head groups and to the self-organization structure of the adsorbed surfactants.

Experimental

I. Experimental details

Materials. Technical grade styrene (styrene, Quimidroga) were used as received. Sodium dodecyl sulfate (>99.5%, Aldrich) was recrystallized from an ethanol/water mixture, potassium persulfate (99%, Aldrich), poly(styrene) (M_w = 280 000 g mol^{-1}, Aldrich) and Disponil AFX 1080 (a 10PEO6PE block copolymer, 80% active content, BASF) were used as received. Doubly deionized water was used throughout the work.

Latex characterization. *Z*-average particle diameters were determined by dynamic light scattering performed on a Malvern Zetasizer ZS using a scattering angle of 173° at a standard temperature of 25 °C. Each measurement was conducted in triplicate and the average of the three values was taken. Conversion was determined gravimetrically.

Latex preparation. Water (757 g), SDS (4 g) and styrene (135 g) were added to a 1 L double walled glass reactor equipped with anchor type stirrer, nitrogen inlet, condenser and thermocouple. The reaction mixture was degassed by nitrogen bubbling for 30 minutes, stirring constantly at 300 rpm, and then heated to 70 °C. Once at reaction temperature, sodium persulfate (225 mg dissolved in 8 g water) was added in a single shot. After 6 hours, the reaction mixture was cooled and filtered through a muslin lining to remove any aggregates. The final conversion of the latex was 96% as determined gravimetrically. The latex was dialyzed until a constant conductivity was obtained. The solids content after dialysis was 13.9 wt% with a mean particle diameter of 76 nm and a polydispersity index (PDI) of 0.07.

Latex soap titration. The CMC and the surface area per molecule (packing area), a_s, of the surfactants were determined by means of surface tension measurements at 23 °C using a Du Noüy ring (KSV Sigma 70, KSV Instruments Ltd) equipped with automatic dosing unit. The diluted latex or DDI water (40 g) were titrated with surfactant solutions measuring the surface tension at various concentration intervals. Multiple measurements at each point were taken and an average was taken.

Quartz crystal microbalance. Polymer coated sensors were obtained by spin coating a solution of poly(styrene) (PS) (M_w = 280 000 g mol^{-1}, 0.5 wt% in toluene) onto a gold sensor (diameter = 14 mm, Q-SENSE, Sweden) at a rate of 50 rps for 1 minute using a Lot Oriel SCC 200 spin coater. The coated thickness was typically 25 nm as measured by difference in frequency before and after coating using the Sauerbrey relationship.[5] The sensors were then placed in an oven at 130 °C for one hour. QCM measurements were performed on a Q-SENSE E1 system operating at 23 °C. Before experiments DDI water was passed over the chip until a stable baseline was obtained. All solutions were passed at a rate of 150 μL min^{-1} using a peristaltic pump. The resonance frequency and dissipation were monitored throughout the experiment at an approximate rate of 1 Hz. Kinetic experiments were conducted by flowing a concentration of surfactant through the QCM for a set period of time (typically 500 seconds). The desorption part of the experiment was then conducted by changing the test solution to deionized water. The QCM-D technique detects changes in the resonance frequency, Δf, and dissipation, ΔD. During the adsorption/desorption cycle the resonance frequency of the crystal changes according to changes in mass. If the mass forms an evenly distributed, rigid layer whose mass is small compared to that of the crystal then the mass per unit area, m, can be calculated from the Sauerbrey equation,[5]

$$\Delta m = \frac{-C\Delta f}{n} \quad (2)$$

where C is a constant (17.7 ng cm^{-2} s^{-1} in this equipment) and n is the resonance overtone number. In this work, n = 5 was used unless otherwise stated. By monitoring the dissipation of the sensor's oscillation, information about the nature of the surface layer can be extracted. The dissipation is defined as,

$$D = \frac{E_{\mathrm{dis}}}{2\pi E_{\mathrm{st}}} \quad (3)$$

where E_{dis} is the energy dissipated during a single cycle and E_{st} is the total energy stored. A large change in D represents a large energy dissipative power of the adsorbed layer and is usually due to thick or less rigid layers. For non-rigid adsorbed layers the Sauerbrey equation results in an underestimation of adsorbed mass since the oscillation of the sensor surface and the film are not fully coupled. In order to account for viscoelastic behavior of the adsorbed layer the Voigt model can be employed using the measured dissipation. To model the viscoelastic properties, four overtones (fifth, seventh, ninth and eleventh) were used and the adsorbed mass calculated using the Voigt model (Q-TOOLS software, Q-Sense, Goeteborg, Sweden). The layer density, fluid viscosity and fluid density were fixed at 1000 kg m^{-3}, 0.001 kg m^{-1} s^{-1}, 1000 kg m^{-3} respectively. The layer viscosity, layer shear and layer thickness were fitted in order to calculate the adsorbed mass.

II. Computational details

Rectangular-shaped boxes, with periodic boundary conditions in all three dimensions, were employed for the simulations. The starting configuration was a pre-equilibrated (for approximately 100 ns) PS slab, placed in the xy-plane, on which surfactants with extended conformation (their long-axis normal, and their tails pointing, to the surface) were arranged in a square lattice. The box lengths in the x- and y-directions were equal and always large enough to ensure absence of interactions of the surfactants with their periodic images. The box length along the normal to the surface direction (z-axis) was elongated to allow a surfactant to be pulled away from the surface to a distance where no effective interactions with either the surface or other surfactants were observed. Then, the region in the simulation box which does not include the PS was filled with water. The resulting systems were subject to a relaxation time of 40 ns and 16 ns for the SDS and PEO–PE surfactants, respectively. Table S1 (ESI†) specifies the details of all systems considered in this work. Note that we choose to present the state of the system by the two-dimensional density, $\rho_{2D} = m/A$, where m is the mass of the surfactants and A is the area of the simulation box in the xy-plane.

The molecular dynamics package GROMACS, version 4.6.5,[6] was used to perform all computer simulations. A temperature of 300 K was maintained by the velocity rescaling thermostat,[7] pertained to the whole system, with a coupling time of 0.1 ps. The pressure in the xy-plane was maintained at 1.0 bar by the Berendsen barostat[8] using a compressibility of 1×10^{-6} bar^{-1} and a coupling time of 1.0 ps, whereas, the box length along the z-axis was fixed. The electrostatic forces were evaluated by the Particle–Mesh–Ewald method[9,10] with a real-space cutoff of 0.9 nm and a grid spacing for the reciprocal-space of 0.12 nm with quadratic interpolation. A 0.9 nm cutoff was also used to calculate the Lennard-Jones potential (with long range dispersion corrections for the energy and pressure). Equilibration stages that did not use constraints were performed with a time step of 2 fs. However, application of the distance constraint within the pull-code (see below) resulted in occasional instabilities. These instabilities disappeared upon reduction of the time step to 1 fs. Thus, whenever the application of a constraint was necessary, a 1 fs time step was used. PS and the surfactants were represented by an explicit-hydrogen all-atom model based on the OPLSAA force-field. In the ESI† we provide a detailed description, Fig. S1–S3 and Tables S2–S4, explanation, and validation of the parameters used. Water molecules were described by the TIP4P-Ew model.[11] Tang *et al.*[12] reported that the structure of the aggregate of 300 or more SDS surfactants at high concentration can depend on the water model used. Therefore, we also performed few simulations of the SDS system with the SPC/E water model.[13] However, we did not observe any substantial difference in the behavior of the surfactants compared with the simulations with the TIP4P-Ew water molecules (see Fig. S7, ESI†). Water bond distances and angles were constrained using the SETTLE algorithm,[14] however, no constraints were applied for the bonded interactions of the surface or surfactant molecules.

Hydrogen bonds were calculated by a donor–acceptor distance cutoff smaller than 0.35 nm and donor–hydrogen–acceptor angle cutoff larger than 150°.[15] Ion contacts were calculated by the sodium–oxygen (of SDS) distance cutoff smaller than the first minimum in the corresponding radial distribution function which was found to be 0.32 nm.

Potentials of mean force calculations. In order to prepare starting conformations for the potential of mean force (PMF), we utilized the pull-code in Gromacs. More specifically, constraint-pulling along the z-axis with cylindrical geometry, was employed with a rate in the range of 1×10^{-4} to 5×10^{-2} nm ps^{-1}. The reference-group was the center of mass of a cylindrical cut of the surface around the pull-vector, and the pull-group was a carbon atom of the hydrophobic tail of the surfactant covalently bonded to the oxygen atom of the hydrophilic head (see Fig. S2 and S3, ESI†). Then, for several chosen distances along the reaction coordinate, we equilibrated the system for a time period in the range of 14 ns to 50 ns (depending on the time the system reached convergence) keeping these distances fixed throughout the simulation. The average force that was required to constrain the distance between the reference and the pull groups was calculated in a data collection step of additional 12 ns. However, at points in which the average force did not exhibit convergence the data collection step was extended to 36 ns. The reason that different points along the reaction coordinate require different equilibration (relaxation) and data-collection times is because of a difference in the interaction of the constrained degree of freedom with its environment. A case in which a longer equilibration time and a longer data collection segment were needed is shown Fig. S4 (ESI†). To obtain the PMF (or free/Gibbs energy profile), this average

force was integrated as a function of the constrained distance, d_c. Because the PMF represents only relative values, it was shifted such that the Gibbs energy of the state at the largest separation corresponds to zero. Furthermore, the distances were also shifted such that the interface between the PS and water is at d_c = 0.0 nm.

The estimation of the errors of the free energy changes were obtained from,[16]

$$\delta\Delta G = \left[\sum_{d_c=0}^{d_{c,max}} (\delta\langle\partial\mathcal{H}/\partial d_c\rangle)^2\right]^{1/2}, \quad (4)$$

where $\mathcal{H}$ is the perturbed Hamiltonian and $\delta\langle\partial\mathcal{H}/\partial d_c\rangle$ is the error in determining the average force at each constrained distance. The value of $\delta\langle\partial\mathcal{H}/\partial d_c\rangle$ was evaluated by the block averaging method.[17]

Results and discussion

Titration and QCM-D experiments

The adsorption isotherms of the anionic surfactant, sodium dodecyl sulfate, and the nonionic Disponil AFX 1080, a 10PEO–6PE block copolymer, were identified experimentally by surface tension measurements using a Du Noüy ring tensiometer. These two surfactants represent typical surfactant systems applied in emulsion polymerization. A thoroughly dialyzed PS latex produced by emulsion polymerization with solids content of 13.9 wt% and average particle diameter of 76 nm was titrated with the two surfactants and the variation in the surface tension with increasing surfactant concentration was observed for several latex particle concentrations (see Fig. 1).

Qualitatively, two key points can be taken from the titration experiments shown in Fig. 1. First, the critical micelle concentration, as determined by the concentration at which the surface tension reaches a constant value in the absence of latex particles, is considerably lower for the nonionic surfactant. The CMC for SDS is 2.3 g L^{-1} while that of Disponil AFX 1080 is 0.05 g L^{-1}. These values are in reasonable agreement with previous experimental studies.[18] Second, for the nonionic surfactant, the presence of even small quantities of latex particles results in significant surfactant adsorption thus resulting in a large difference in the measured surface tension for a given amount of surfactant added. This behavior can be analyzed quantitatively from the adsorption isotherms which can be derived based on the assumption that a given surface tension value of the air–water interface is directly related to the equilibrium surfactant concentration in the aqueous phase, $[S]_{aq}$. Assuming that the amount of surfactant adsorbed at the air–water interface is negligible compared with the amount adsorbed on the latex particles (due to the large difference in the surface area of both interfaces), from a mass balance, the total surfactant concentration [S], is equal to the sum of $[S]_{aq}$ and the amount of adsorbed emulsifier,

$$[S] = [S]_{aq} + \Gamma\frac{A_p}{V_{aq}} \quad (5)$$

where A_p is the total surface area of the latex particles, V_{aq} is the volume of the aqueous phase and Γ is the amount of adsorbed emulsifier per unit area of latex. The value of $[S]_{aq}$ can be calculated from the curves in Fig. 1 from the value of the air–water surface tension and interpolation of the curve in the absence of latex, assuming that a given surface tension corresponds to a given $[S]_{aq}$. The value of Γ can be calculated accordingly. This analysis allows the construction of the adsorption isotherms shown in Fig. 2.

The isotherms for the two surfactants were fit either to the Langmuir isotherm (Disponil AFX 1080),

$$\Gamma = \Gamma_\infty\frac{K[S]_{aq}}{1 + K[S]_{aq}}, \quad (6)$$

or the Frumkin isotherm[19] (SDS),

$$\frac{\Gamma/\Gamma_\infty}{1 - \Gamma/\Gamma_\infty}e^{[2a\cdot\Gamma/\Gamma_\infty]} = K[S]_{aq}, \quad (7)$$

where Γ_∞ is the maximum quantity of surfactant that can be adsorbed, K is the adsorption constant and a is an adjustable parameter associated with molecular interactions. The use of the Frumkin isotherm was necessary for the SDS data as it

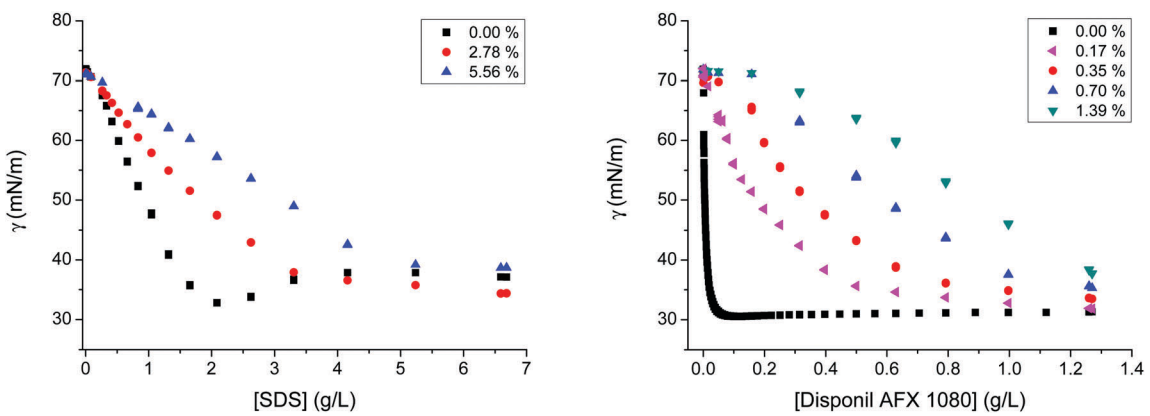

Fig. 1 Variation of surface tension with increasing bulk concentration of SDS and Disponil AFX 1080 for different solid content of the poly(styrene) latex as shown in the figure legends.

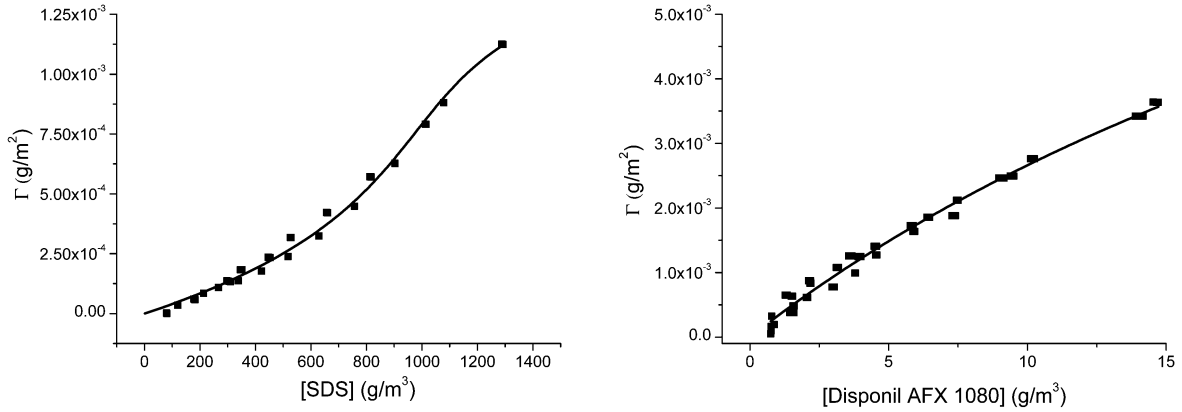

Fig. 2 Adsorption isotherms of SDS and Disponil AFX 1080 onto poly(styrene). Lines represent fit of the experimental data to the Langmuir or Frumkin isotherm as detailed in the text.

Table 1 Estimated values of the parameters obtained from fit of the modified Langmuir isotherm to the data shown in Fig. 2

	K [m^3 mol^{-1}]	a_{CMC} [Å^2]
SDS	0.064 ± 0.002	29 ± 5
Disponil AFX 1080	7.4 ± 1.2	24 ± 9

shows a more S-like pattern which is not accounted for by the standard Langmuir isotherm indicating some cooperativity in the adsorption profile, as has previously been observed for the adsorption of SDS on hydrophobic polymer surfaces.[20–22]

A summary of the resulting equilibrium constants and packing area of the surfactant molecules at the PS surface at the CMC a_{CMC} are shown in Table 1. The value of a_{CMC} was calculated from eqn (6) or (7) using a value of $[S]_{aq}$ equal to the CMC of each surfactant. It is clear that the equilibrium constant for the nonionic surfactant is significantly higher than that of SDS, in agreement with previous experimental data.[21,23,24] In both cases the absolute value of a_{CMC} is slightly lower than some previous experimental results using polystyrene surfaces obtained by spin-coating and scattering techniques to measure surfactant adsorption.[25] However, measurements using latex particles have given values similar to those reported here for the adsorption of SDS on polystyrene surfaces, suggesting that surface roughness in polymer latexes may result in an underestimation of the total surface area and consequently affect estimates of a_{CMC} and K. For example, Brown and Zhao[26] conducted experiments using polystyrene latex particles of 200 nm and found a packing area of 30 Å^2 which compares very favorably with our results. They also observed a very similar adsorption isotherm to that of the present case with a tendency to increase the strength of adsorption with increasing surface density. For the non-ionic surfactant the lack of literature data makes comparison difficult but in comparison to other PEO–PE surfactants which typically have area of 50–70 Å^2 the value obtained here seems significantly lower.[27–30] One possible reason for this is that PEO–PE surfactants typically contain a broad distribution of chain lengths with varying numbers of ethylene glycol units. Small quantities of molecules with very few ethylene glycol units can have a huge impact on adsorption behavior. For example, Turner *et al.* showed that the presence of residual dodecanol in recrystallized SDS results in a measurement of almost twice the surface concentration compared to highly purified SDS.[25]

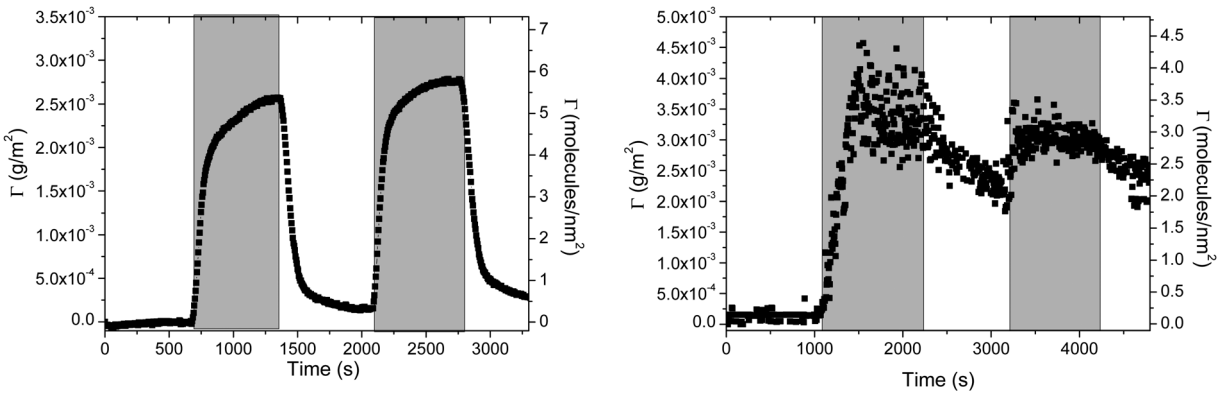

Fig. 3 Adsorption of SDS (left panel) and Disponil AFX 1080 (right panel) onto poly(styrene) measured by QCM-D. Initially water is flown through the cell followed by two cycles of either SDS (1.8 g L^{-1}) or Disponil AFX 1080 (0.02 g L^{-1}). Shaded regions correspond to time periods in which the surfactant solution is being passed over the polymer surface.

One important point that has been highlighted recently is how the strength of surfactant adsorption can also impact on nucleation events in emulsion polymerization.[21,24] In order to further explore this and to investigate the reversibility of surfactant adsorption at varying concentrations the QCM-D technique was used. The QCM equipment is capable of measuring small changes in surface concentration and was used in a series of experiments in which a PS surface was sequentially subjected to water and surfactant solution to monitor adsorption and desorption from the surface. In order to convert the measured change in frequency to a mass per unit area the Sauerbrey relation was used, which is based on the assumption that the adsorbed surfactant layer is rigid. Whilst for SDS this assumption is valid, as confirmed by the similar values obtained for the amount of surfactant adsorbed in comparison to the surface tension measurements shown in Fig. 2, for the non-ionic surfactant, the PEO part of the chain is hydrated and therefore leads to viscoelastic behavior of the adsorbed layer. In this case the mass adsorbed was calculated using the Voigt model which takes into account the viscoelasticity through the relationship of the measured frequency and energy dissipation at a number of resonance frequencies.

Fig. 3 shows the plot of the amount of surfactant adsorbed to the surface with time when subjected to surfactant solution (shown in grey areas), at around the CMC of each surfactant, and water. It can be observed that after adsorption, SDS is rapidly removed from the surface when the surfactant solution is replaced with water. In the case of the nonionic surfactant, however, upon flowing water through the cell the surfactant is very slow to be removed. Previous work has shown that this is a common occurrence for nonionic surfactants when adsorbed to polymer surfaces and was previously attributed to the a change in the strength of adsorption as a function of the surface coverage of the surfactant such that at low concentration the nonionic surfactant is strongly bound.[24]

Potentials of mean force calculations

In order to explain the experimental observations we studied the strength and nature of surfactant adsorption at polymer surfaces using molecular dynamics simulations. The strength of the adsorption was calculated by measuring the Gibbs (free) energy required to pull a surfactant adsorbed at the PS–water interface to the bulk water phase. In order to display the behavior of the systems at equilibrium (thus, at zero pull-force and when all surfactants are adsorbed) for the different 2D-densities studied, we plot in Fig. 4 the density profiles normal to the PS–water interface. As expected, the hydrophilic

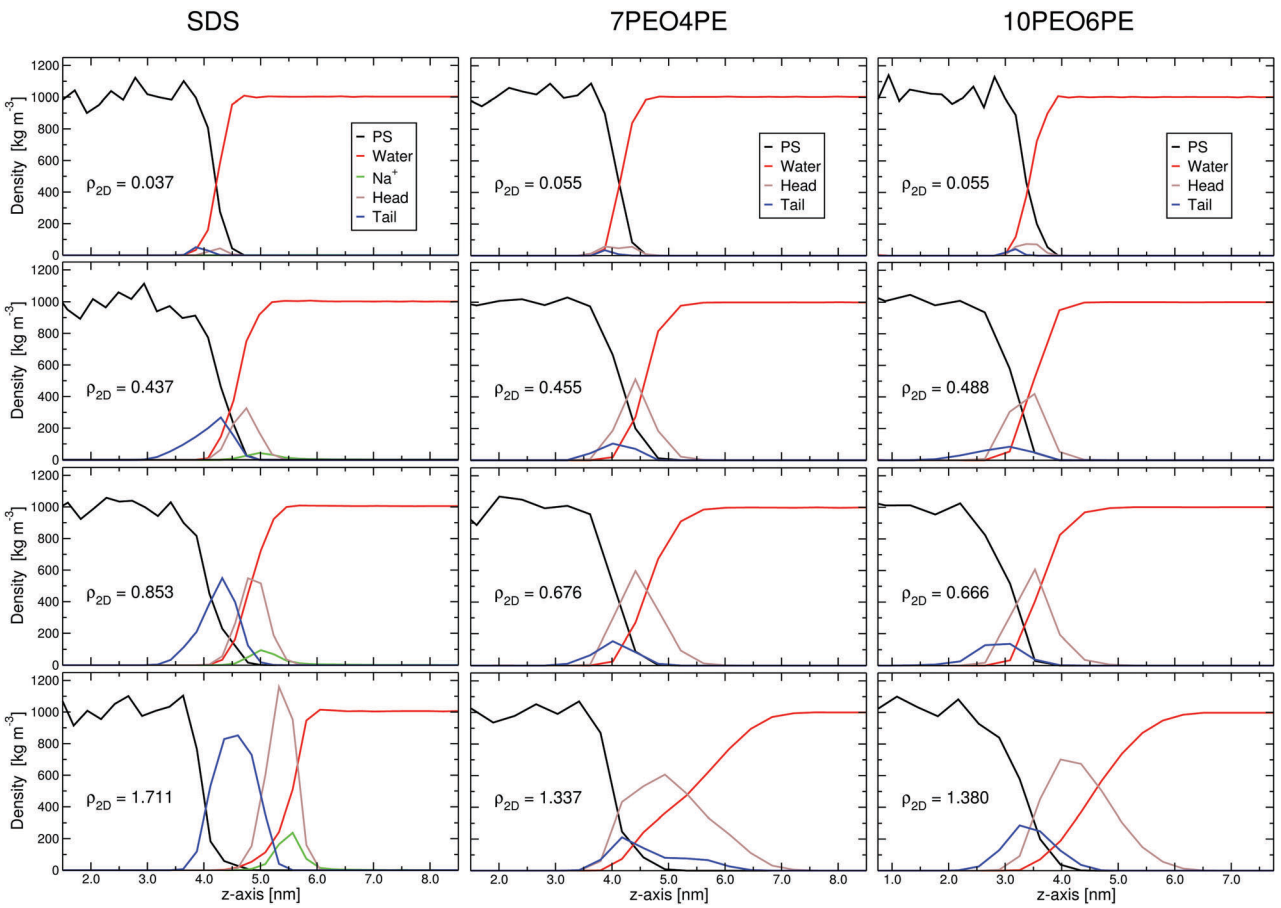

Fig. 4 Density profiles perpendicular to the PS–water interface at different surfactant two-dimensional densities. Left, middle and right panels are for SDS, 7PEO4PE and 10PEO6PE surfactants, respectively. Each surfactant is divided into a hydrophilic head and a hydrophobic tail as defined in Fig. S2 and S3 (ESI†). Only part of the simulation box around the interface is shown.

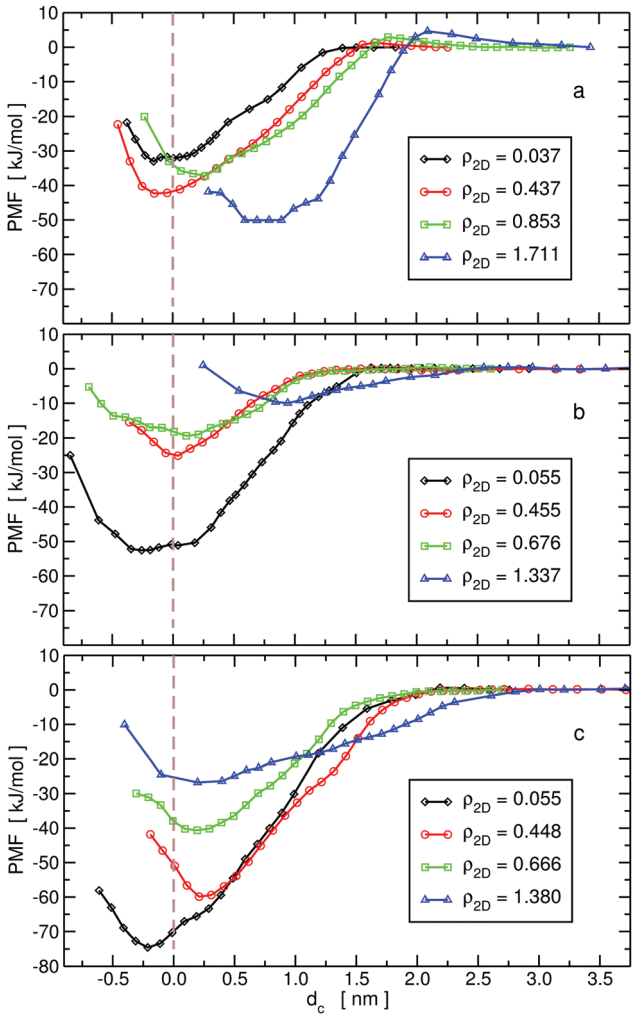

Fig. 5 The potential of mean force of pulling away one surfactant from the poly(styrene)–water interface into the water phase as a function of the constrained distance, d_c (see Experimental section for details). The different curves correspond to different 2D-densities, indicated in mg m^{-2}, of the surfactant adsorbed at the interface. Panel (a) is for SDS, (b) for 7PEO4PE, and (c) for Disponil AFX 1080 (10PEO6PE) surfactants. The brown vertical dashed line marks to the PS–water interface.

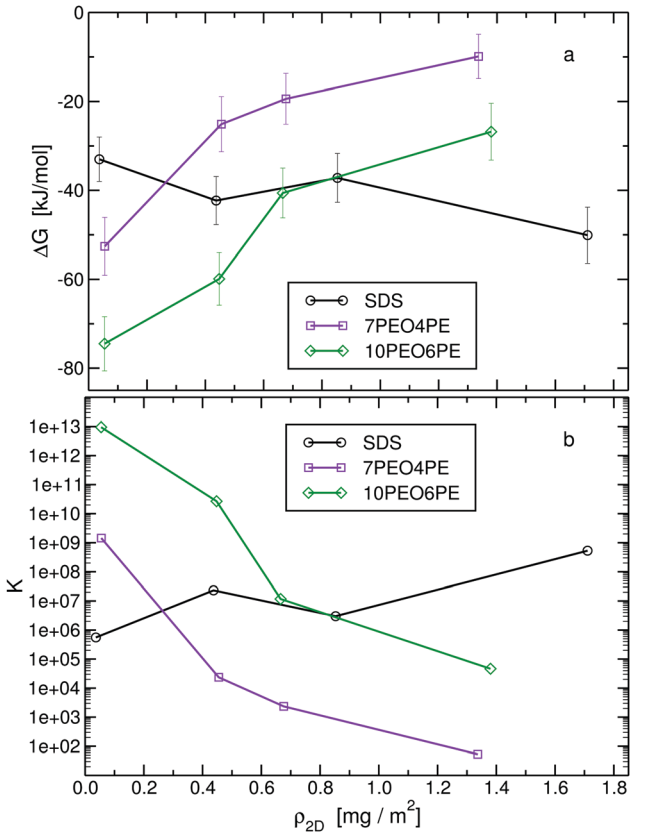

Fig. 6 (a) The Gibbs (free) energy change, and (b) the corresponding equilibrium constant at T = 300 K, for the adsorption process of the different surfactants at the poly(styrene)–water interface for different 2D-densities of the adsorbed surfactants.

head of the surfactants points toward the water phase whereas the hydrophobic tail points toward, and to some extent penetrates, the PS surface. For SDS, the water–PS interface is sharp (*i.e.*, the two phases share a small overlapping region) for all densities. However, for the non-ionic surfactants at high 2D-densities, the variation in the water density is more gradual.

In Fig. 5 we display the free energy profiles (potentials of mean force (PMF)) of removing one surfactant adsorbed to the surface. A clear distinction between ionic and non-ionic surfactants is observed. In the former, the strength of adsorption of SDS moderately increases with the increase of 2D-density (with a minor deviation in the trend between ρ_{2D} = 0.437 mg m^{-2} and ρ_{2D} = 0.853 mg m^{-2}). In contrast, in the case of the two non-ionic surfactants, a considerably stronger force (more negative free energy) is required to pull a surfactant away from the surface as its 2D-density decreases. In addition at low concentrations of 10PEO6PE, the magnitude of the free energy is substantially larger than that of SDS, despite the fact that both have the same length of hydrocarbon tail. Both observations are in agreement with the experimental results shown in Fig. 3 which indicate the process of washing-out the surfactants is slower, and the removal of the last surfactants (*i.e.* at low concentrations) from the surface is more difficult for 10PEO6PE than for SDS. It should, however, be noted that the QCM experiments are affected by both the thermodynamic equilibrium of surfactant adsorption/desorption, and the kinetic processes of surfactant removal, and diffusion away from, the polymer surface. The shape of the PMF curves we obtained for these systems, as well as for other systems involving extended surfaces,[31] suggests that at least for low concentrations the free energy barrier for adsorption is either very low or practically nonexistent. Therefore, the depth of the potential-well is also a measure for the free energy barrier from which the kinetics of the desorption processes can be derived.[32,33] As an exception for this, we point-out that at high concentrations, steric interactions and the need for surface reorganization may lead to slower adsorption kinetics than is reflected in the PMF.

The free energy change of adsorbing the surfactant from the water phase to the surface as a function of its 2D-density is shown in Fig. 6a. The qualitatively different behavior is

reflected by the positive slopes for the non-ionic surfactants *versus* the mild negative slope for the ionic surfactant. The values of the Gibbs energy change upon binding can be converted to equilibrium constants using the relation, $K = \exp^{-\Delta G/RT}$, which are shown for $T = 300$ K in Fig. 6b. Note however, that a direct quantitative comparison with values obtained from the experiment is not possible because the equation for the adsorption process and, thereby, the corresponding expression and dimension of the equilibrium constant are different.[34,35] The models used experimentally consider the surface as composed of adsorbing sites with a total concentration equals to Γ_∞. In contrast, in the simulations the surface is treated as a region in space to which the surfactants can migrate without explicitly entering the equilibrium expression.

Properties of the layers from by the adsorbed surfactants

Why do the nonionic surfactants experience substantial strengthening, whereas SDS (a moderate) weakening, in their adsorption to the PS surface with decreasing density? To address this question we first consider the direct interactions of the surfactants with the surface. In Fig. S5 (ESI†), we exhibit this interaction which indicates that in all cases, the surfactant-surface attraction becomes stronger with decreasing surfactant concentration by a roughly similar slope. This can be explained by the fact that at low concentrations, the long-axis of the surfactant aligns parallel to the surface plane. As the density increases, the surfactant long-axis tends to adopt a more perpendicular orientation (Fig. S6, ESI†), thereby, losing considerable contact (and as a consequence the interaction energy) with the surface. Thus, the direct surfactant-surface interaction energy can be ruled-out as the reason for the contrasting behavior. In the following we will argue that a significant contribution for this behavior lies in the structure of the assembly of the surfactants at the surface and the properties of the head group.

The driving force for a surfactant in aqueous solution to adsorb at hydrophobic/hydrophilic interface is predominantly the minimization of the hydrophobic water-exposed surface area of its tail and the surface. The interaction is thus solvent-induced and for the size of hydrophobic tail relevant to this study (large-scale regime), the adsorption process is driven by favorable changes in enthalpy and entropy.[31,36] Nevertheless upon adsorption of surfactants, there is a loss of favorable interactions between the head group and the aqueous solution which are compensated by the reduction in the interaction between the hydrophobic surface and water. The magnitude of this loss depends on the conformation of the surfactant as well as on its environment at the interface, and therefore, can display variations with changes in the concentration of adsorbed surfactants. In Table 2 we present the total number of hydrogen bonds in the system for the adsorbed state relative to the desorbed state.

In the majority of the cases, the values are positive due to a reduction in the number of water molecules surrounding the surfactants or the PS surface (or equivalently, due to an increase in the number of water molecules in the bulk phase) which form a smaller number of hydrogen bonds relative to bulk waters. For the non-ionic surfactants, the excess number of hydrogen bonds in the adsorbed state decreases with increasing concentration. It starts from positive values at low concentrations and changes sign at the highest concentration. For the ionic surfactant, no such reduction is observed. The variations are small except at the highest density where an increase is displayed. This increase is, however, likely to be a result of changes in the distributions of the counter-ions (see below).

Table 2 The change in the number of hydrogen bonds in the entire system for the adsorption process of a single surfactant, at different surfactant concentrations, as defined in the reaction coordinate for the PMFs

# of surfactants	SDS	7PEO4PE	10PEO6PE
1	+0.9 ± 0.8	+2.4 ± 0.8	+4.4 ± 0.7
8	—	+2.1 ± 1.0	+2.6 ± 1.2
12	+0.2 ± 0.7	+0.2 ± 1.2	+0.9 ± 1.4
24	+0.9 ± 0.7	−0.2 ± 1.3	−2.6 ± 1.1
48	+3.9 ± 0.7	—	—

Where does the reduction in the number of hydrogen bonds for the adsorption process of the non-ionic surfactants arise from? Fig. 7 displays the last configuration for the simulations with the highest density for the three surfactants. The SDS molecules are assembled perpendicular, with a slight tilt, to the surface. The assembly is ordered where the tails interact with one another and the heads interact with the water molecules and the sodium ions. The interaction with sodium ions also counter-balance the electrostatic repulsions between the head groups. In contrast, the non-ionic surfactants form a disordered assembly and the head and tail groups do not segregate due to an interwoven configuration (see also Fig. 4), a behavior in accord with experimental findings.[37] In Fig. S8 (ESI†) we plot for the nonionic surfactants the head–tail radial distribution functions (excluding intra-molecule interactions). The behavior of the curves for the first neighbor shell atoms ($r \lesssim 0.7$ nm) suggests that the degree of interweaving is slightly larger for the shorter surfactant (7PEO4PE) and that it displays a maximum as the surfactants 2D-density increases. It is interesting to point that based on reflectometry studies on the kinetics of nonionic surfactants it was suggested that at high concentration, ''the surfactant molecules stagger in the interface such that there is a possible overlap of hydrophilic headgroups with hydrophobic tails''.[29] Furthermore, proton nuclear magnetic resonance relaxation investigations demonstrated that nonionic surfactants containing PEO display a high degree of flexibility.[38] Anyway in both the long and short nonionic surfactants considered in our simulations, not all of the oxygens of the PEO heads are surrounded by molecules able to donate them a hydrogen because a significant number of these oxygens are in contact with other head groups or with the PE tails.‡ Thus, these head group oxygen atoms are not able to satisfy all their hydrogen-bond forming capacity. This partial loss of the ability

‡ Note that only the terminal hydroxyl group of the head groups and the water molecules are able to donate a hydrogen, however, hydrogen bonds between the surfactants are found to be insignificant in number.

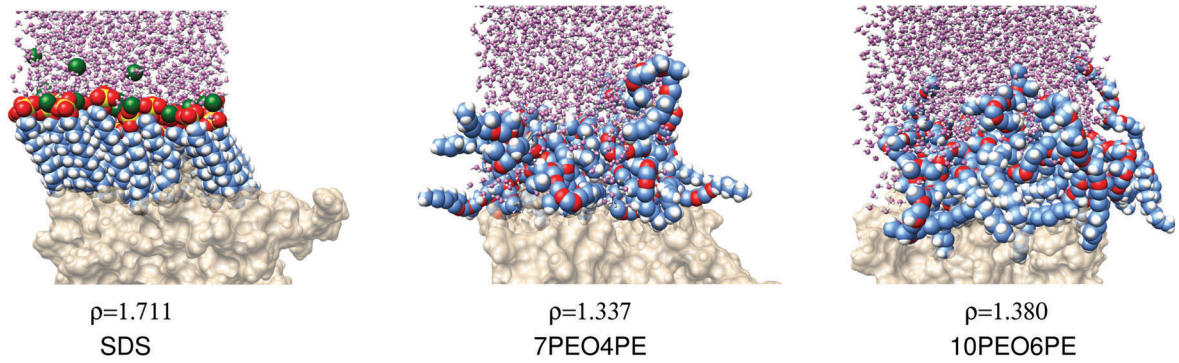

Fig. 7 Snapshots of the simulation box showing the assembly of the surfactants at the interface. Poly(styrene) molecules are represented by a surface representation in beige, water molecules (oxygens in purple and hydrogens in white) in a ball-and-stick model, sodium ions as green spheres, and the surfactant (carbon in blue, hydrogens in white, oxygens in red, and sulfur in yellow) in a space-filling model.

to form hydrogen bonds, which is heightened by the increase of the 2D-density (and partially explains the trend observed in Table 2 for non-ionic surfactants), will decrease the driving force of the surfactant to adsorb at the interface.

In order to quantify this effect we proceed to examine the interaction between the head groups of the surfactants and the entire system. However, in the case of SDS we note that as the 2D-density of the surfactant increases, the concentration of the sodium ions in the vicinity of (and in contact with) these heads groups increases as well, a phenomenon reminiscent, albeit with a smaller magnitude, of multivalent counterion condensation.[39–42] This is shown in Fig. S9a (ESI†) by the radial distribution functions (RDFs) of the head group oxygen atoms with the oxygen of water. A decrease in the height of the first peak is observed, which indicates reduced contacts and thereby reduced hydrogen bondings. Nevertheless, the lost hydrogen bondings with the water molecules are replaced by contacts with the sodium cations (displayed in the RDFs in Fig. S9b, ESI†)

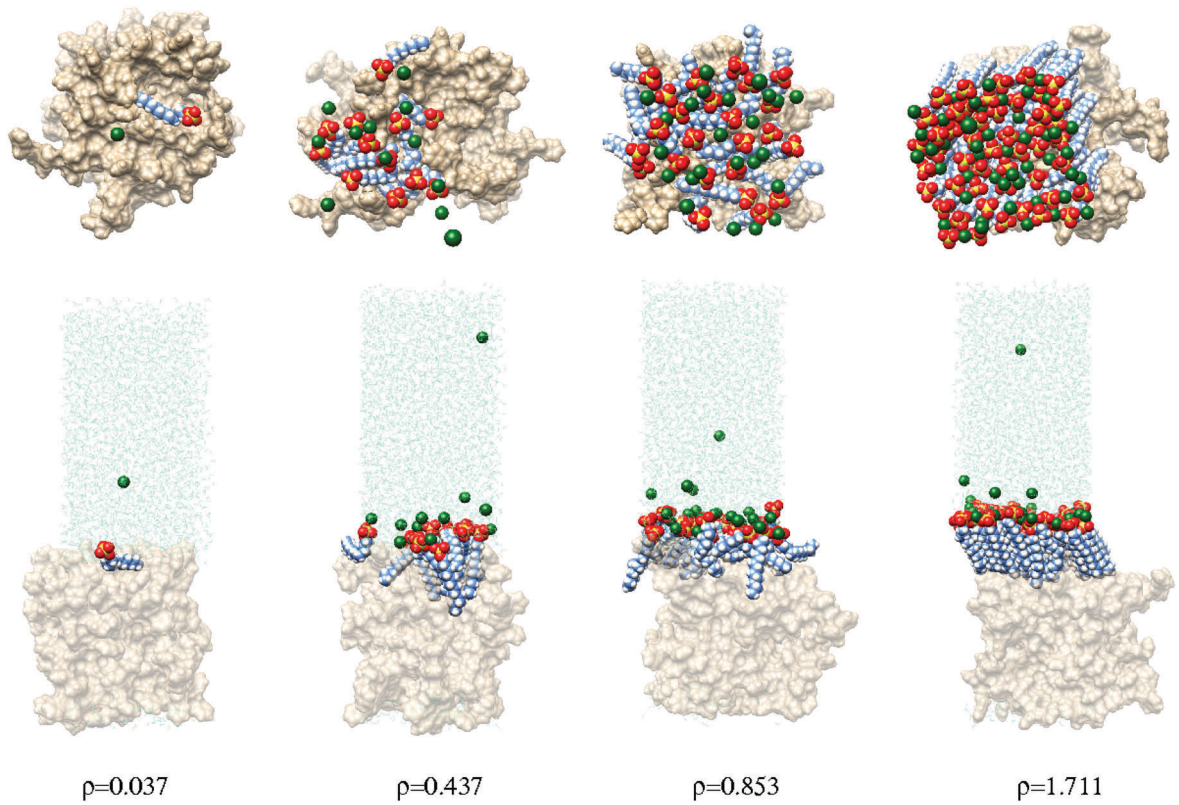

Fig. 8 Top-view (upper panel) and side-view (lower panel) of instantaneous configuration of the simulations box of the SDS surfactants adsorbed at the interface (*i.e.* at equilibrium) for different 2D-densities given in mg m^{-2}. Sodium cations are shown as green spheres, the poly(styrene) in a surface representation colored beige, and water molecules are colored in light-blue in a wire-frame representation. Note that the molecules are not broken due to periodic boundary conditions and the figures do not capture the entire length of the box along the *z*-axis (normal to the surface).

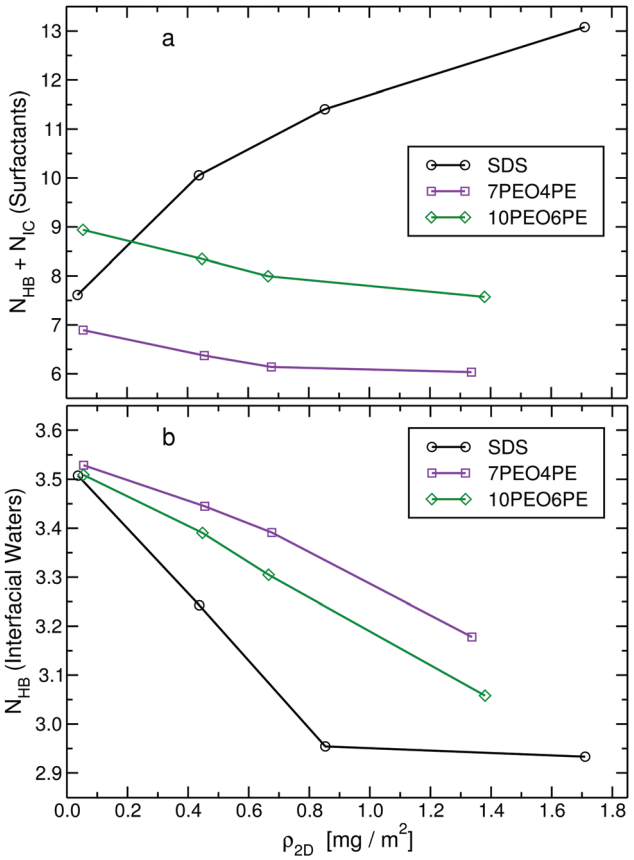

Fig. 9 (a) The number of hydrogen bonds and ion contacts, between the surfactants and the system, per surfactant. (b) The number of hydrogen bonds, per water molecule, the (intruding/interfacial) II-waters make with the system. The II-waters were determined as the first 400 waters closest to the surfactants tails. Both figures are analyzed for the adsorbed state and are plotted as a function of the 2D-density.

resulting in a gain of electrostatic interactions which also allows to overcome the repulsion between the charged head groups. Snapshots of the SDS surfactants at the interface are shown in Fig. 8. Thus for SDS, the interaction of the heads groups with the surrounding solvent molecules must also include the sodium cations.

In Fig. 9a we calculate the number of hydrogen bonds, and where relevant, also the number of ion contacts, between the surfactants and the entire system (for SDS a decomposition of the total number is shown in Fig. S10, ESI†). For the non-ionic surfactants a decrease in the number of hydrogen bonds is observed as the density is increased. This confirms the physical picture described above of the decline in the ability of the oxygen atoms of the PEO segments to accept hydrogen bonds. The number of hydrogen bonds, per surfactant, lost for the entire density range studied is 0.9 and 1.4 for the 7PEO4PE and 10PEO6PEO, respectively. For SDS, however, the sum of hydrogen bonds and ion-contacts exhibits an increase with increasing density, largely due to the behavior of the sodium ions.

Furthermore, the impaired structure of the layer formed by the nonionic surfactants affects not only the surfactants themselves but also the surrounding water molecules. In the density profiles shown in Fig. 4 we note that at high concentrations, the curve for water at the interface with nonionic surfactants does not decreases sharply as it does in the case of SDS. This is due to water molecules intruding the surfactant layer and forming hydrogen bonds with the oxygen atoms of PEO as shown in Fig. 7. Obviously, this helps to stabilize the surfactant, however, at the expense of the stability of the intruding waters. In bulk, a water molecule is surrounded by four other water molecules and at room temperature forms on average 3.5 hydrogen bonds.[43] However, when they penetrate the surfactant layer they are not able to maintain this number of hydrogen bonds.

In order to identify these penetrating waters, we calculate the minimum distance between all waters and any atom of the tail group of all surfactants. Then, we consider the first 400§ water molecules closest to the tails. Nevertheless, for the lowest concentration these waters correspond to water molecules at the interface and to hardly any intruding waters. In Fig. 9b we plot the number of hydrogen bonds formed by these water molecules, hereafter, referred to as (intruding/interfacial) II-waters. For the non-ionic surfactants, a linear decrease with increasing surfactant density is observed, supporting the argument of the loss of interaction energy of the II-waters. Fig. 10 shows a zoom of the interface layer for the long non-ionic surfactant. It clearly demonstrates that the intruding waters and the oxygens of the PEO segment of the surfactants form incomplete hydrogen-bond interactions.

For SDS the decrease is sharper at low densities and it seems to plateau at higher densities (nevertheless, additional densities in this region are needed to validate that it is indeed a plateau). In this case, the II-waters are predominantly interfacial and the reduction in the number of hydrogen bonds they experience is due to an increase in the concentration of the sodium counter-ions (characterized by a relatively high-charge density) at the interface.[43] These drastic changes of the electrostatic interactions in the system for SDS, which mainly compensate each other, are associated with large fluctuations in the energy. This unfortunately, impede us from drawing further conclusions on the adsorption of the ionic surfactant to the surface.

Concerning the effect of entropy and especially that originating from the flexibility of the surfactant chains, we note that in addition to the orientational preference of the long axis of the surfactants, Fig. S6 (ESI†) indicates that the end-to-end distance of the PEO–PE surfactants increases with concentration whereas that of SDS hardly changes (as expected from their different persistence lengths[44,45]). Such straightening of the PEO–PE chains reduces their entropy and thereby contributes to their weakened adsorption with increasing concentration. Nevertheless, it is not the only factor affecting the Gibbs adsorption energy because the curves in Fig. S6 (ESI†) do not mirror the changes in the adsorption free energy shown in Fig. 6. Furthermore, from additional simulations we conducted

§ This number was estimated to be the number of water molecules penetrating the non-ionic surfactant layer in the simulations with the highest 2D-density.

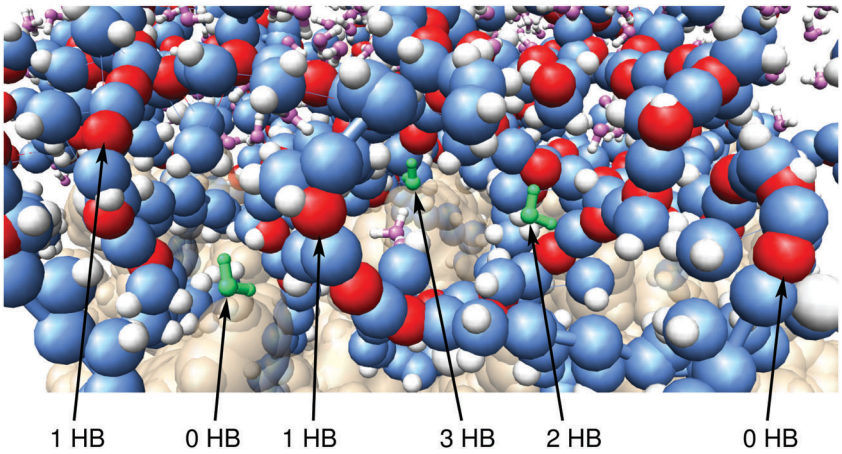

Fig. 10 A close-up of the structure of the 10PEO6PE non-ionic surfactant layer on the poly(styrene) surface at ρ_{2D} = 1.380 mg m^{-2}. The six arrows point to three waters (colored in green) and to three surfactant oxygens and the corresponding number of hydrogen bonds these waters/oxygens make with the entire system is indicated.

of the same nonionic surfactants but with artificially stiff dihedral angles (see description in the ESI,† Fig. S11 and S12) we obtained that the reduction of the chains flexibility was accompanied also by a loss in the degree of interweaving heads and tails groups (Fig. S13, ESI†), as well as, by a loss in the ability of the surfactants to hydrogen bond with the water molecules (Fig. S5, ESI†).

Conclusions

Surfactants in aqueous solutions favorably adsorb to hydrophobic surfaces in order to minimize the hydrophobic solvent exposed area of their tails and the surface. Normally, it is assumed that upon adsorption the interactions of the head groups with the solvent are not substantially affected. However, in this work we find that this is not the case, especially for nonionic surfactants with aprotic head groups such as poly(ethylene oxide). This conclusion, together with the explanation we provide for the contrasting behavior of ionic and non-ionic surfactants, critically relies on two observations obtained from the simulations. The first is that there is a large degree of interweavement between head and tail groups in the adsorbed layer formed by the non-ionic surfactant (PEO/PE systems). The second is that water molecules penetrate this layer.

In the disordered layer these nonionic surfactants generate at the surface, only oxygens of the head groups present at the interface with the water phase or oxygens next to penetrating waters can form hydrogen bonds. Oxygens inside this layer lose this favorable energy, with a magnitude that increases with the surfactants density at the interface. This reduced stability of the surfactants diminishes their driving force for adsorption. That means, the effective interaction of the surfactant with the surface increases with the decrease in their concentration. This behavior is shown to be in accordance with experimental results on the dynamics of surfactant desorption, which indicated that at low surface concentrations non-ionic surfactants are very slow to desorb from the surface. In the case of the ionic surfactant this behaviour is not observed. In this case, SDS assembles into an ordered structure and the attraction to the surface was even slightly augmented at higher surfactant concentrations, in agreement with the experimentally determined adsorption isotherm. We hypothesize, that the reason these two types of surfactants behave differently is because the ionic surfactant has a small head group that is strongly hydrophilic, whereas, the head groups of the nonionic surfactants are large and only weakly attracted to water.

Acknowledgements

Diputación Foral de Gipuzkoa, University of the Basque Country UPV/EHU (UFI 11/56), Basque Government (GVIT373-10) are gratefully acknowledged for their financial support. We would like to thank the technical and human support of the computer cluster provided by IZO-SGI SGIker of UPV/EHU and European funding (ERDF and ESF).

References

1 J. W. Gibbs, On the equilibrium of heterogeneous substances, *Trans. Conn. Acad. Arts Sci.*, 1878, **3**, 343–524.
2 W. D. Harkins, A General Theory of the Mechanism of Emulsion Polymerization, *J. Am. Chem. Soc.*, 1947, **69**, 1428–1444.
3 R. G. Gilbert, *Emulsion Polymerization: A Mechanistic Approach*, Colloid Science, Academic Press, London, 1995.
4 S. C. Thickett and R. G. Gilbert, Emulsion polymerization: state of the art in kinetics and mechanisms, *Polymer*, 2007, **48**, 6965–6991.
5 G. Sauerbrey, Verwendung von Schwingquarzen zur Wägung dünner Schichten und zur Mikrowägung, *Z. Phys.*, 1959, **155**(2), 206–222.
6 B. Hess, C. Kutzner, D. van der Spoel and E. Lindahl, GROMACS 4: Algorithms for Highly Efficient, Load-Balanced, and Scalable Molecular Simulation, *J. Chem. Theory Comput.*, 2008, **4**, 435–447.

7 G. Bussi, D. Donadio and M. Parrinello, Canonical Sampling through Velocity Rescaling, *J. Chem. Phys.*, 2007, **126**, 014101.
8 H. J. C. Berendsen, J. P. M. Postma, W. F. van Gunsteren, A. DiNola and J. R. Haak, Molecular Dynamics with Coupling to An External Bath, *J. Chem. Phys.*, 1984, **81**, 3684–3690.
9 T. Darden, D. York and L. Pedersen, Particle Mesh Ewald: An N-log(N) Method for Ewald Sums in Large Systems, *J. Chem. Phys.*, 1993, **98**, 10089–10092.
10 U. Essmann, L. Perera, M. L. Berkowitz, T. Darden, H. Lee and L. G. Pedersen, A Smooth Particle Mesh Ewald Method, *J. Chem. Phys.*, 1995, **103**, 8577–8593.
11 H. W. Horn, W. C. Swope, J. W. Pitera, J. D. Madura, T. J. Dick, G. L. Hura and T. Head-Gordon, Development of an improved four-site water model for biomolecular simulations: TIP4P-Ew, *J. Chem. Phys.*, 2004, **120**, 9665–9678.
12 X. Tang, P. H. Koenig and R. G. Larson, Molecular Dynamics Simulations of Sodium Dodecyl Sulfate Micelles in Water – The Effect of the Force Field, *J. Phys. Chem. B*, 2014, **118**, 3864–3880.
13 H. J. C. Berendsen, J. R. Grigera and T. P. Straatsma, The missing term in effective pair potentials, *J. Phys. Chem.*, 1987, **91**, 6269–6271.
14 S. Miyamoto and P. A. Kollman, SETTLE: An Analytical Version of the SHAKE and RATTLE Algorithms for Rigid Water Models, *J. Comput. Chem.*, 1992, **13**, 952–962.
15 A. Luzar and D. Chandler, Structure and hydrogen bond dynamics of water–dimethyl sulfoxide mixtures by computer simulations, *J. Chem. Phys.*, 1993, **98**, 8160–8173.
16 E. Guàrdia, R. Rey and J. A. Padró, Statistical Errors in Constrained Molecular Dynamics Calculations of the Mean Force Potential, *Mol. Simul.*, 1992, **9**, 201–211.
17 H. Flyvbjerg and H. G. Petersen, Error Estimates on Averages of Correlated Data, *J. Chem. Phys.*, 1989, **91**, 461–466.
18 P. Mukerjee and K. J. Mysels, *Critical Micelle Concentrations of Aqueous Surfactant Systems*, U.S. National Bureau of Standards, Washington, DC, 1971.
19 M. I. Volkova-Gugeshashvili, A. G. Volkov and V. S. Markin, Adsorption at Liquid Interfaces: The Generalized Frumkin Isotherm and Interfacial Structure, *Russ. J. Electrochem.*, 2006, **42**, 1073–1078.
20 H. M. Vale and T. F. McKenna, Adsorption of sodium dodecyl sulfate and sodium dodecyl benzenesulfonate on poly(vinyl chloride) latexes, *Colloids Surf., A*, 2005, **268**, 68–72.
21 L. L. Hecht, A. Schoth, R. Muñoz-Espí, A. Javadi, K. Köhler, R. Miller, K. Landfester and H. P. Schuchmann, Determination of the Ideal Surfactant Concentration in Miniemulsion Polymerization, *Macromol. Chem. Phys.*, 2013, **214**, 812–823.
22 W. Brown and J. Zhao, Adsorption of Sodium Dodecyl Sulfate on Polystyrene Latex Particles using Dynamic Light Scattering and Zeta Potential Measurements, *Macromolecules*, 1993, **26**, 2711–2715.
23 D. Colombié, K. Landfester, E. D. Sudol and M. S. El-Aasser, Competitive Adsorption of the Anionic Surfactant SLS and the Nonionic Surfactant Triton X-405 on Polystyrene Latex Particles, *Langmuir*, 2000, **16**, 7905–7913.
24 N. Ballard, J. Urrutia, S. Eizagirre, T. Schäfer, G. Diaconu, J. C. de la Cal and J. M. Asua, Surfactant Kinetics and Their Importance in Nucleation Events in (Mini)emulsion Polymerization Revealed by Quartz Crystal Microbalance with Dissipation Monitoring, *Langmuir*, 2014, **30**, 9053–9062.
25 S. F. Turner, S. M. Clarke, A. R. Rennie, P. N. Thirtle, D. J. Cooke, Z. X. Li and R. K. Thomas, Adsorption of Sodium Dodecyl Sulfate to a Polystyrene/Water Interface Studied by Neutron Reflection and Attenuated Total Reflection Infrared Spectroscopy, *Langmuir*, 1999, **15**, 1017–1023.
26 J. W. Brown and W. H. Huestis, Structure and orientation of a bilayer-bound model tripeptide. A ^{1}H NMR study, *J. Phys. Chem.*, 1993, **97**, 2967–2973.
27 J. Zhao and W. Brown, Dynamic Light Scattering Study of Nonionic Surfactant ($C_{12}E_{25}$) Adsorption on Polystyrene Latex Particles: Effect of Poly(ethylene oxide) Chain Size, *J. Phys. Chem.*, 1996, **100**, 5908–5912.
28 B. R. Postmus, F. A. M. Leermakers, L. K. Koopal and M. A. Cohen Stuart, Competitive Adsorption of Nonionic Surfactant and Nonionic Polymer on Silica, *Langmuir*, 2007, **23**, 5532–5540.
29 C. Geffroy, M. A. Cohen Stuart, K. Wong, B. Cabane and V. Bergeron, Adsorption of Nonionic Surfactants onto Polystyrene: Kinetics and Reversibility, *Langmuir*, 2000, **16**, 6422–6430.
30 J. R. Lu, Z. X. Li, R. K. Thomas, E. J. Staples, L. Thompson, I. Tucker and J. Penfold, Neutron Reflection from a Layer of Monododecyl Octaethylene Glycol Adsorbed at the Air–Liquid Interface: The Structure of the Layer and the Effects of Temperature, *J. Phys. Chem.*, 1994, **98**, 6559–6567.
31 R. Zangi, Driving Force for Hydrophobic Interaction at Different Length-Scales, *J. Phys. Chem. B*, 2011, **115**, 2303–2311.
32 H. A. Kramers, Brownian Motion in a Field of Force and the Diffusion Model of Chemical Reactions, *Physica*, 1940, **7**, 284–304.
33 S. J. Hagen, Solvent Viscosity and Friction in Protein Folding Dynamics, *Curr. Protein Pept. Sci.*, 2010, **11**, 385–395.
34 Y. Liu, Is the Free Energy Change of Adsorption Correctly Calculated?, *J. Chem. Eng. Data*, 2009, **54**, 1981–1985.
35 X. Zhou and X. Zhou, The Unit Problem in the Thermodynamic Calculation of Adsorption Using the Langmuir Equation, *J. Chem. Eng. Data*, 2014, **201**, 1459–1467.
36 K. Lum, D. Chandler and J. D. Weeks, Hydrophobicity at small and large length scales, *J. Phys. Chem. B*, 1999, **103**, 4570–4577.
37 J. R. Lu, T. J. Su, Z. X. Li, R. K. Thomas, E. J. Staples, I. Tucker and J. Penfold, Structure of Monolayers of Monododecyl Dodecaethylene Glycol at the Air–Water Interface Studied by Neutron Reflection, *J. Phys. Chem. B*, 1997, **101**, 10332–10339.
38 C. Boissier, J.-E. Löfroth and M. Nydén, Water-Based Latex Dispersions. 2. Adsorption and Dynamics of Nonionic Surfactants on Colloidal Particles with Different Interfacial Properties, *Langmuir*, 2002, **18**, 7313–7319.
39 G. S. Manning, Limiting Laws and Counterion Condensation in Polyelectrolyte Solutions I. Colligative Properties, *J. Chem. Phys.*, 1969, **51**, 924–933.

40 A. Mukherjee, K. Schmitz and L. Bhuiyan, Overcharging in macroions. Effects of macroion geometry/charge distribution, *Langmuir*, 2003, **19**, 9600–9612.
41 K. Besteman, M. A. G. Zevenbergen and S. G. Lemay, Charge inversion by multivalent ions: dependence on dielectric constant and surface-charge density, *Phys. Rev. E: Stat., Nonlinear, Soft Matter Phys.*, 2005, **72**, 061501.
42 Z. Li, A. K. V. Dyk, S. J. Fitzwater, K. A. Fichthorn and S. T. Milner, Atomistic Molecular Dynamics Simulations of Charged Latex Particle Surfaces in Aqueous Solution, *Langmuir*, 2016, **32**, 428–441.
43 R. Zangi, Can Salting-In/Salting-Out Ions be Classified as Chaotropes/Kosmotropes?, *J. Phys. Chem. B*, 2010, **114**, 643–650.
44 L. J. Magid, Z. Li and P. D. Butler, Flexibility of Elongated Sodium Dodecyl Sulfate Micelles in Aqueous Sodium Chloride: A Small-Angle Neutron Scattering Study, *Langmuir*, 2000, **16**, 10028–10036.
45 H. Lee, R. M. Venable, A. D. MacKerell and R. W. Pastor, Molecular Dynamics Studies of Polyethylene Oxide and Polyethylene Glycol: Hydrodynamic Radius and Shape Anisotropy, *Biophys. J.*, 2008, **95**, 1590–1599.

Electronic Supplementary Material (ESI) for Soft Matter.

Supplementary Information:

Adsorption Behavior of Ionic and Nonionic Surfactants on Polymer Surfaces

Giulia Magi Meconi[1], Nicholas Ballard[1], José M. Asua[1], and Ronen Zangi[2,3]

[1]POLYMAT & Departamento de Química Aplicada, Facultad de Ciencias Químicas, University of the Basque Country UPV/EHU, Avenida de Tolosa 72, 20018, Donostia–San Sebastián, Spain

[2]POLYMAT & Departamento de Química Orgánica I, University of the Basque Country UPV/EHU, Avenida de Tolosa 72, 20018, Donostia–San Sebastián, Spain

[3]IKERBASQUE, Basque Foundation for Science, María Díaz de Haro 3, 48013 Bilbao, Spain

October 19, 2016

Table S1: Details of the simulation setups for the three surfactants studied. For each surfactant we considered four concentrations reported as two-dimensional densities, ρ_{2D}. The molecule, 16-mer PS, composing the surface is defined in Fig. S1. The average length of the simulation box along each axis is also shown.

	# Surfactants	ρ_{2D} [mg/m^2]	# 16-mer PS	# Waters	$\langle X \rangle / \langle Y \rangle$ [nm]	$\langle Z \rangle$ [nm]
SDS	1 / 12 / 24 / 48	0.0365 – 1.71	20	2853 – 2973	3.62 – 3.67	10.71 – 12.11
7PEO4PE	1 / 8 / 12 / 24	0.0551 – 1.34	20	3491 – 6560	3.58 – 3.64	12.10 – 20.07
10PEO6PE	1 / 8 / 12 / 24	0.0545 – 1.38	22	3949 – 11417	4.25 – 4.37	9.37 – 22.05

A Model for Poly(styrene)

A PS chain is modeled as a 16-mer unit. Because the stereochemistry of each unit is randomly generated during polymerization, we chose to model each chain with alternating C_α chiral centers (R followed by S). The bonded and non-bonded parameters of PS were taken from the OPLS-AA model of ethylbenzene[1,2]. However, in order to allow the connectivity between the subunits and simultaneously maintain zero charge for each of these subunits, we made the following changes. The partial charge of C_β of the first residue was changed from -0.180 to -0.120, that of C_γ of the last residue was changed from -0.115 to -0.055, and both changes were applied to the repeating residues. The resulting model is shown in Fig. S1 and the non-bonded interactions are specified in Table S2. Using this model, we obtained a value of 1.02 kg/m^3 for the density of amorphous PS which is close to its experimental value[3] of 1.04–1.06 kg/m^3. Furthermore, the calculated values of the radius of gyration, 9.8 Å, and the weight-normalized end-to-end distance squared, 0.42 Å$^2\cdot$ mol/g, are also in a very good agreement with their experimentally determined values of 10.0 Å and 0.43 Å$^2\cdot$ mol/g, respectively, as well as with other models for PS[4–6].

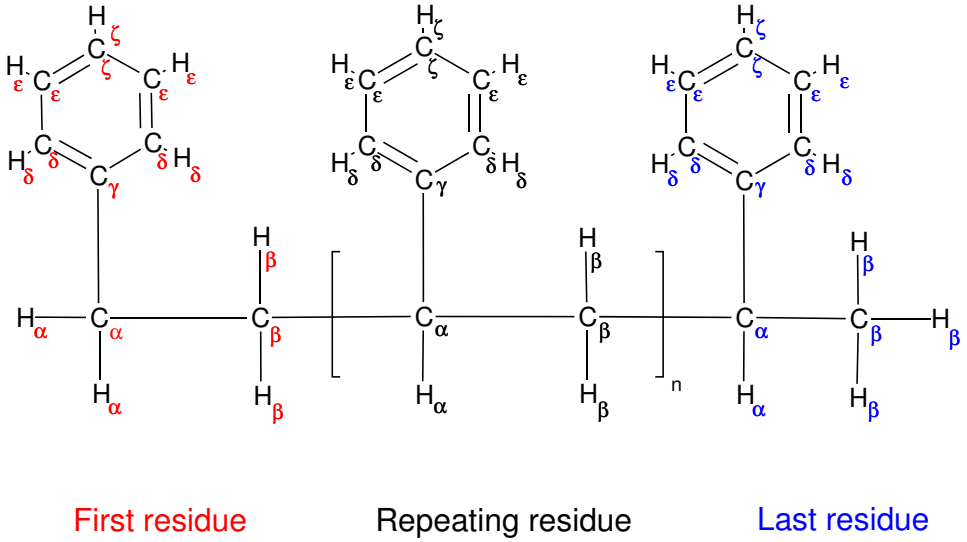

Figure S1: The model for poly(styrene) based on the OPLS-AA force-field. The partial charge and LJ parameters describing each atom is detailed in Table S2. Note that the C_α of the repeating and last residues are chirals, nevertheless, the parameters for the R and S configurations are the same.

Table S2: Partial charges and LJ parameters for the poly(styrene) model. The values refer to all residue types (first, repeating, and last) unless otherwise indicated.

	q [e]	σ [nm]	ϵ [kJ/mol]
C_α	-0.005	0.350	0.276
C_β	-0.120	0.350	0.276
$C_{\beta,\text{last}}$	-0.180	0.350	0.276
C_γ	-0.055	0.355	0.293
$C_{\gamma,\text{first}}$	-0.115	0.355	0.293
H_α, H_β	+0.060	0.250	0.126
C_δ, C_ϵ, C_ζ	-0.115	0.355	0.293
H_δ, H_ϵ, H_ζ	+0.115	0.242	0.126

A Model for Sodium Dodecyl Sulfate

Bonded and nonbonded parameters for SDS were adopted from the model of Shelley et al.[7,8]. However, because this model integrates the hydrogens of the methyl and methylene groups into the carbons to which they are connected, we performed quantum calculations, following the RESP (Restrained Electrostatic Potential) charge fitting procedure[9], to determine the partial charges in these groups. Bonded interactions that were missing for the all-atom description were taken from the corresponding interactions of the OPLS-AA force-field. The resulting model is displayed in Fig. S2 and the non-bonded parameters in Table S3 The LJ parameters of the sodium counterion, σ=0.333 nm and ϵ=0.0116 kJ/mol, were taken from the OPLS-AA force-field.

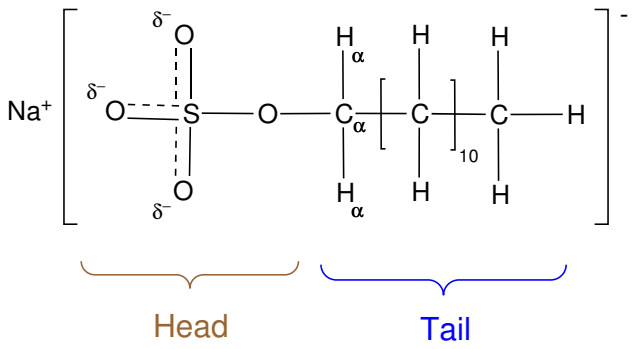

Figure S2: The model for SDS surfactant. The partial charge and LJ parameters describing each atom is detailed in Table S3.

Table S3: Partial charges and LJ parameters for the SDS model. The atoms are divided according to their association to the head or tail groups.

	q [e]	σ [nm]	ϵ [kJ/mol]
Head			
S	+1.284	0.355	1.046
O	-0.654	0.315	0.837
O_{ester}	-0.459	0.300	0.711
Tail			
C_α	+0.077	0.350	0.276
H_α	+0.030	0.242	0.063
C	-0.120	0.350	0.276
C_{last}	-0.180	0.350	0.276
H	+0.060	0.250	0.126

A Model for poly(ethylene oxide)-poly(ethylene)

For the PEO-PE surfactant, we considered molecules with two different lengths. The shorter surfactant, labeled as 7PEO4PE, is $HO-(CH_2CH_2O)_7-(CH_2)_7-CH_3$. The longer surfactant, labeled as 10PEO6PE, is $HO-(CH_2CH_2O)_{10}-(CH_2)_{11}-CH_3$ to which Disponil AFX1080 was compared experimentally. Results from a self-consistent field theory predicts that the head size of the surfactant influences the adsorption significantly[10]. Parameters for the PE and PEO segments of the surfactant were taken from the OPLS-AA force-field[11]. For the latter, the values were derived from dimethyl ether group. The model for this surfactant is given in Fig. S3 and Table S4.

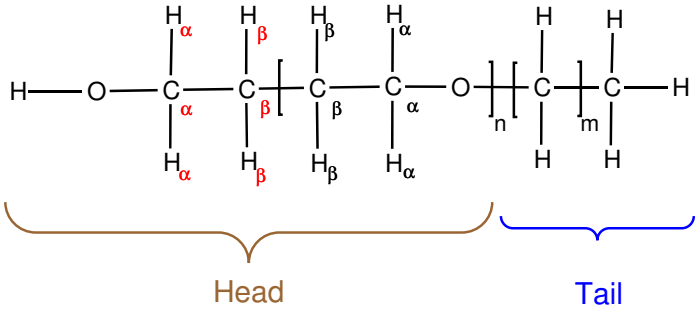

Figure S3: The model for PEO-PE surfactant. The partial charge and LJ parameters describing each atom is detailed in Table S4.

Table S4: Partial charges and LJ parameters for the PEO-PE surfactant model. The atoms are divided according to their association to the head or tail groups.

	q [e]	σ [nm]	ϵ [kJ/mol]
Head			
$C_{\alpha,\beta}$	+0.140	0.350	0.276
$C_{\alpha,\text{first}}$	-0.015	0.350	0.276
$H_{\alpha,\beta}$	+0.030	0.250	0.126
$H_{\alpha,\text{first}}$	+0.040	0.250	0.126
O	-0.400	0.290	0.586
O_{first}	-0.683	0.312	0.711
H_{first}	+0.418	0.000	0.000
Tail			
C	-0.120	0.350	0.276
C_{last}	-0.180	0.350	0.276
H	+0.060	0.250	0.126

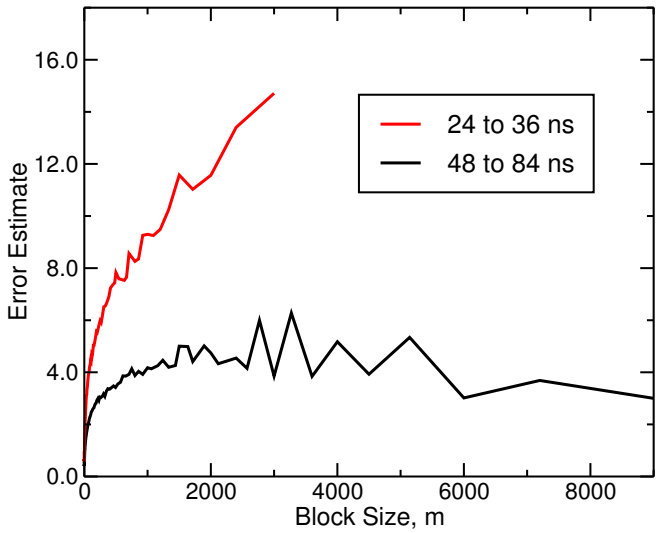

Figure S4: Analysis of the convergence of the constrained force along different segments of the trajectory for 10PEO6PE with 24 surfactants at d_c=0.103 nm. This point is in the vicinity of the equilibrium adsorbed state and convergence required longer simulation. In order to obtain an estimate for the error we used the block averaging method. The trajectory is divided into n number of blocks of equal size m and averages are calculated for each block. The error for the total average is calculated from the variance between the averages of the n blocks. The curves show this error estimate as a function of the block size m. The plot for the earlier and shorter segment of the trajectory (24–36 ns) continues to increase as the block size increases (or the number of blocks decreases) whereas the last and longer segment of the trajectory (48–84 ns) exhibits a plateau (and even a slight decrease due to sufficient number of blocks which are large enough) which signifies convergence.

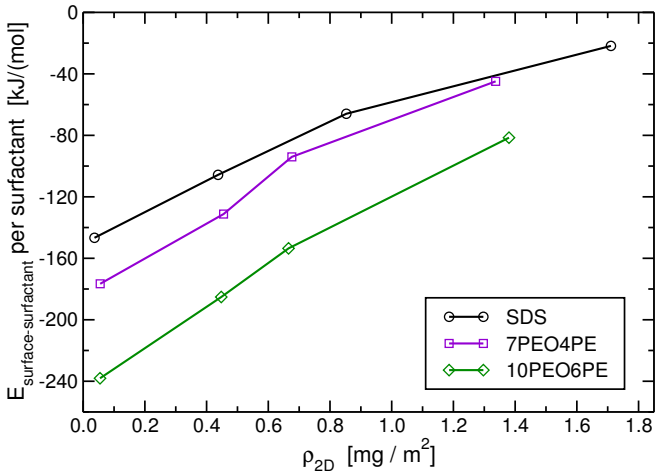

Figure S5: The surface-surfactant energy per surfactant as a function of the 2D-density.

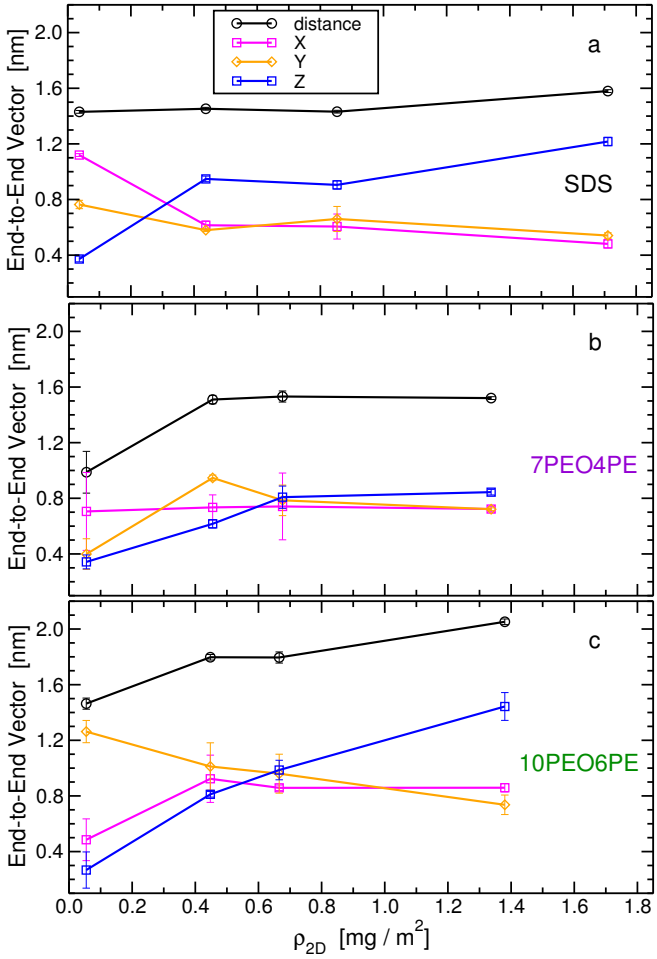

Figure S6: The end-to-end vector of the surfactant (between the heavy atoms at both ends) as a function of the 2D-density. The plots show the scalar distance as well as the projections parallel (x and y) and normal (z) to the interface plane. This analysis is performed for the equilibrium points (adsorbed state) of the pulling processes shown in Fig. 5 averaged over the last 36 ns of the trajectories. Error bars are displayed, however, in some cases their size is comparable to the size of the symbols.

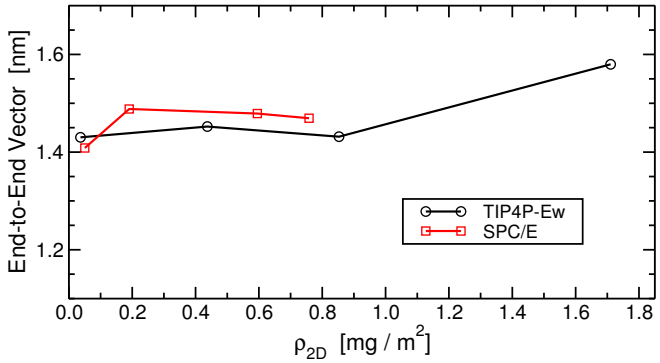

Figure S7: Comparison of the end-to-end distance (between the heavy atoms at both ends) of the SDS surfactants from simulations in which the water molecules were described by the TIP4P-Ew and SPC/E water models.

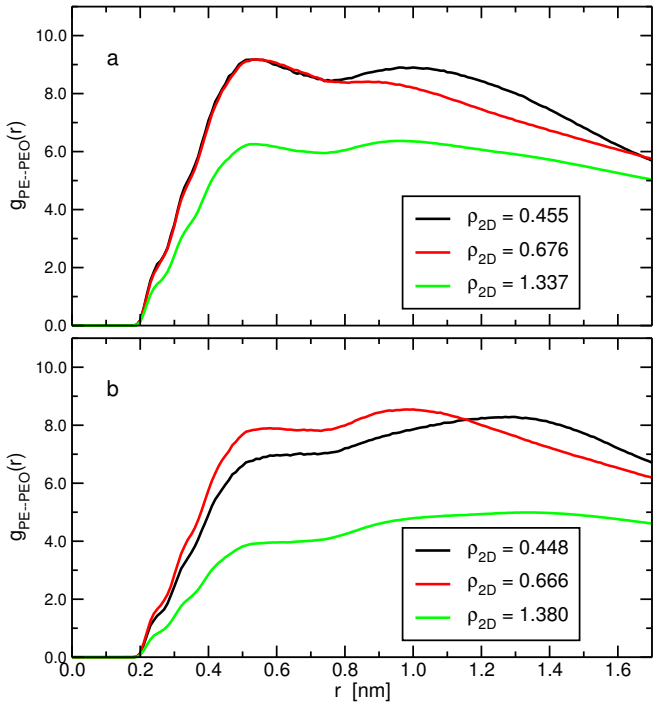

Figure S8: The radial distribution functions between the tail atoms (the PE segment) and head atoms (the PEO segment excluding the connecting –CH_2CH_2O– group) of different surfactants for different 2D-densities for the (a) 7PEO4PE and (b) 10PEO6PE systems. The analyzes are computed for the equilibrium points of the pulling processes shown in Fig. 5 averaged over the last 36 ns of the trajectories.

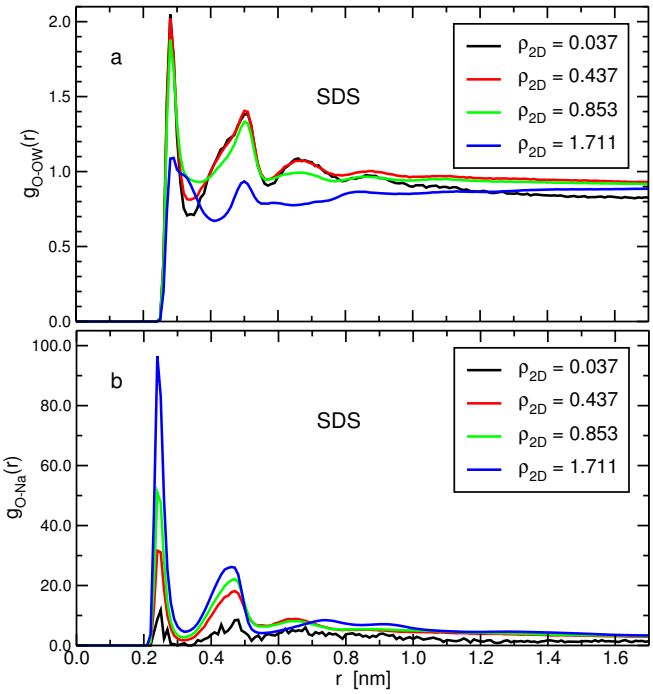

Figure S9: The radial distribution functions between the oxygen atoms of SDS and (a) the oxygen atoms of water, (b) the sodium cations, at different two-dimensional densities. The analyzes are computed for the equilibrium points (adsorbed state) of the pulling processes shown in Fig. 5 averaged over the last 36 ns of the trajectories.

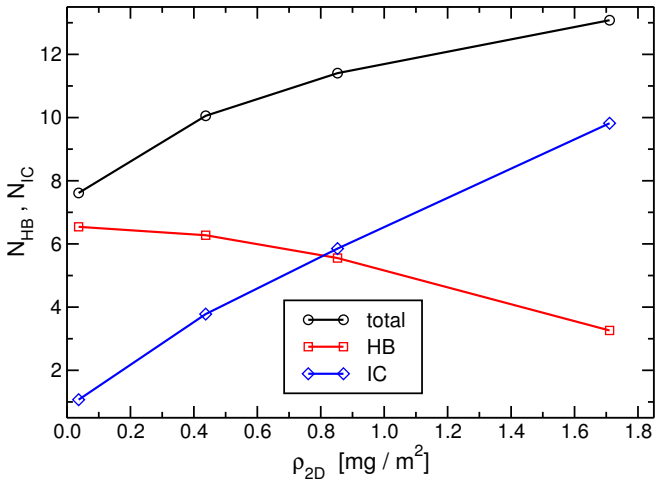

Figure S10: The number of hydrogen bonds and the number of ion contacts, per surfactant, between SDS molecules and the solvent as a function of the 2D-density. The analysis is performed in the adsorbed state.

The Effect of the Chain Stiffness

In order to investigate the effect of the stiffness of the nonionic surfactants on the structure of the adsorbed layer at the interface with the PS surface, we performed additional simulations for the long and short surfactants in which their dihedral angles were characterized by a much stiffer potentials ($V_d = k_\phi [1 + \cos(n\phi)]$ with k_ϕ=10 kJ/mol, ϕ=180 °, and n=3). For each system we considered 12 surfactants in exactly the same conditions as with the unperturbed systems except for the number of water molecules which were 4300 and 10500 for the 7PEO4PE and 10PEO6PE surfactants, respectively. The resulting 2D-densities were ρ_{2D}=0.681 and 0.702 mg/m^2 which are to be compared with the ρ_{2D}=0.666 and 0.676 mg/m^2 of the unperturbed OPLS-AA force-field for the short and long surfactants, respectively. The simulations were run in the adsorbed state for 100 ns and data were collected for 36 ns.

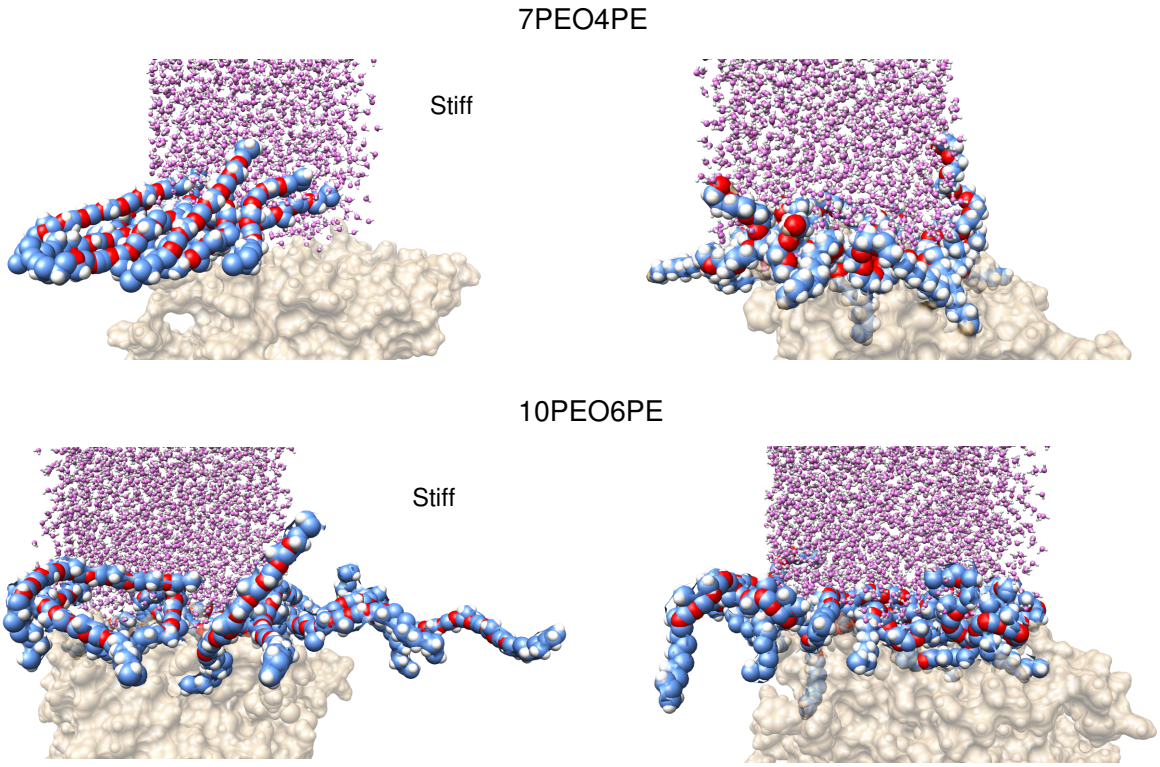

Figure S11: Snapshots from the simulations with the stiff nonionic surfactants described above (left panel) compared with those with unperturbed OPLSAA force field (right panel).

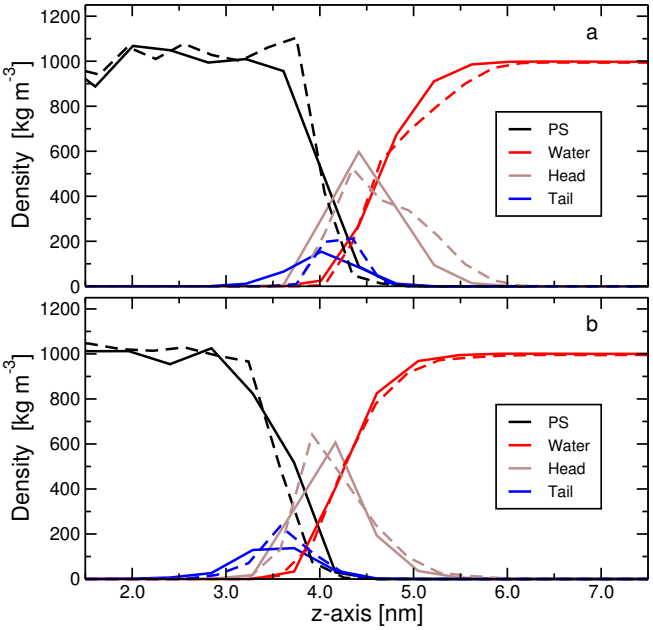

Figure S12: The density profiles of the system with the stiff (dashed lines) nonionic surfactants compared with those with the unperturbed OPLSAA force-field (solid lines) for the (a) 7PEO4PE and (b) 10PEO6PE systems. The profiles were superimposed on top of each other in such a way to maximize the overlap of the curves for the water phase.

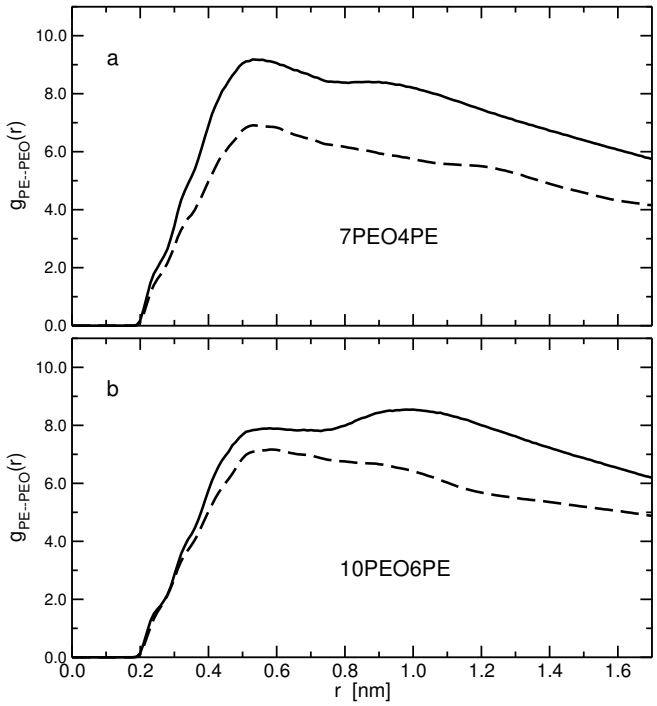

Figure S13: The radial distribution functions between the tail atoms (the PE segment) and head atoms (the PEO segment excluding the connecting $-CH_2CH_2O-$ group) of different surfactants for the system with stiff (dashed lines) nonionic surfactants compared with those with unperturbed OPLSAA force-field (solid lines) for the (a) 7PEO4PE and (b) 10PEO6PE systems.

Table S5: The end-to-end distance, as well as its three components, of the surfactants with the stiff dihedral angles compared to those with the unperturbed dihedrals. In the last row we provide the number of hydrogen bonds, per surfactant, between the surfactants (head groups) and the water molecules.

	7PEO4PE		10PEO6PE	
End-to-End	stiff	unperturbed	stiff	unperturbed
distance	2.03	1.53	2.33	1.80
X	1.10	0.74	1.43	0.86
Y	1.23	0.79	1.34	0.96
Z	0.99	0.81	1.02	0.99
HB	5.0	6.1	6.2	7.9

References

[1] Jorgensen, W. L.; Severance, D. L. Aromatic-Aromatic Interactions: Free Energy Profiles for the Benzene Dimer in Water, Chloroform and Liquid Benzene, *J. Am. Chem. Soc.* **1990**, *112*, 4768–4774.

[2] Price, M. L. P.; Ostrovsky, D.; Jorgensen, W. L. Gas-Phase and Liquid-State Properties of Esters, Nitriles, and Nitro Compounds with the OPLS-AA Force Field, *J. Comp. Chem.* **2001**, *22*, 1340–1352.

[3] Brandrup, J.; Immergut, E. H.; Grulke, E. A. *Polymer Handbook;* Wiley: New York, fourth ed., 2003.

[4] Fetters, L. J.; Lohse, D. J.; Richter, D.; Witten, T. A.; Zirkel, A. Connection between Polymer Molecular Weight, Density, Chain Dimensions, and Melt Viscoelastic Properties, *Macromolecules* **1994**, *27*, 4639–4647.

[5] Harmandaris, V. A.; Adhikari, N. P.; van der Vegt, N. F. A.; Kremer, K. Hierarchical Modeling of Polystyrene: From Atomistic to Coarse-Grained Simulations, *Macromolecules* **2006**, *39*, 6708–6719.

[6] Spyriouni, T.; Tzoumanekas, C.; Theodorou, D.; Müller-Plathe, F.; Milano, G. Coarse-Grained and Reverse-Mapped United-Atom Simulations of Long-Chain Atactic Polystyrene Melts: Structure, Thermodynamic Properties, Chain Conformation, and Entanglements, *Macromolecules* **2007**, *40*, 3876–3885.

[7] Shelley, J.; Watanabe, K.; Klein, M. L. Simulation of a sodium dodecylsulfate micelle in aqueous solution, *Int. J. Quant. Chem.* **1990**, *38*, 103–117.

[8] Schweighofer, K. J.; Essmann, U.; Berkowitz, M. Simulation of Sodium Dodecyl Sulfate at the Water-Vapor and Water-Carbon Tetrachloride Interfaces at Low Surface Coverage, *J. Phys. Chem. B* **1997**, *101*, 3793–3799.

[9] Bayly, C. I.; Cieplak, P.; Cornell, W.; Kollman, P. A. A well-behaved electrostatic potential based method using charge restraints for deriving atomic charges: the RESP model, *J. Phys. Chem.* **1993**, *97*, 10269–10280.

[10] Jódar-Reyes, A. B.; Ortega-Vinuesa, J. L.; Martín-Rodríguez, A.; Leermakers, F. A. M. Self-Consistent Field Model of Inhomogeneous Adsorption of Nonionic Surfactants onto Polystyrene Latex, *Langmuir* **2003**, *19*, 878–887.

[11] Jorgensen, W. L.; Maxwell, D. S.; .; Tirado-Rives, J. Development and Testing of the OPLS All-Atom Force Field on Conformational Energetics and Properties of Organic Liquids, *J. Am. Chem. Soc.* **1996**, *118*, 11225–11236.